Hindawi
Shock and Vibration
Volume 2021, Article ID 6655694, 12 pages
https://doi.org/10.1155/2021/6655694

Research Article

Sliding Impact Mechanism of Square Roadway Based on Complex Function Theory

Decheng Ge,[1] Fuxing Jiang,[1] Cunwen Wang,[2] Yang Chen,[3] Chunyu Dong,[2] Sitao Zhu,[1] Zhaoyi Wang,[4] and Fei Han[2]

[1]*School of Civil and Resource Engineering, University of Science and Technology Beijing, Beijing 100083, China*
[2]*Research Center for Rock Burst Control of Shandong Energy Group Co., Ltd., Jinan, Shandong 250014, China*
[3]*Shandong Energy Group Co., Ltd., Jinan, Shandong 250014, China*
[4]*Liangbaosi Coal Mine, Shandong Energy Feicheng Mining Group Co., Ltd., Jining, Shandong 272400, China*

Correspondence should be addressed to Cunwen Wang; wangcunwen@snjt.com

Received 13 December 2020; Revised 7 January 2021; Accepted 20 January 2021; Published 31 January 2021

Academic Editor: Yuantian Sun

To clarify the process of stress change and plastic zone evolution of square roadways under high-stress conditions, the rotational square expansion plastic zone evolution model of square roadway was established by theoretical analysis, numerical simulation, and engineering verification. The shear slip impact stress criterion of square roadway based on complex variable function theory was studied, and the law of surrounding rock stress distribution, plastic zone expansion, elastic energy density, local energy release rate (LERR), and total energy release of square roadway were analyzed. The results show that the compressive stress is concentrated in the four corners of the roadway after the roadway excavated and transfers with the change of plastic zone. Main shear failures start from the four corners and develop in a rotating square shape, forming square failure zones I and II. The square failure zone I is connected with the roadway contour and rotated 45°. The square failure zone II is connected with the square failure zone I and rotated 45°. When the original rock stress is low, the surrounding rock tends to be stable after the square shear slip line field formed. When the original rock stress is high, the shear failure of the surrounding rock continues to occur after the square failure zone II formed, showing a spiral slip line. Corners of the square roadway and square failure zones I and II are the main energy accumulation and release areas. The maximum elastic energy density and LERR increase exponentially with the ratio of vertical stress to uniaxial compressive strength (*Ic*). When square corners of the roof are changed to round corners, the plastic zone of the roof expands to form an arch structure. The maximum elastic energy density decreases by 22%, which reduces the energy level and possibility of rock burst. This study enriches the failure mechanism of roadway sliding impact. It can provide a basic theoretical reference for the design of the new roadway section and support form based on the prevention of rock burst.

1. Introduction

The causes of rock burst are various, and their manifestations are also different [1–4]. The cross section of many premining roadways in a coal mine is square or rectangular, and a lot of rock burst happened in these roadways. For example, on February 22, 2020, a rock burst occurred in Xinjulong Coal Mine, resulting in four deaths and extensive roadway damage. Many scholars have studied the failure of rectangular and square roadways and achieved fruitful results.

Shi et al. [5] studied the stress distribution law of rectangular roadways under different span height ratios and lateral pressure coefficients. Guo et al. [6] studied the evolution law of plastic zone and large-scale failure criterion of roadway surrounding rock by FLAC numerical simulation method. Wu et al. [7, 8] found that V-shaped belt failure occurred on both sides of the tunnel through

true triaxial experiment and numerical simulation. Wang et al. [9] established the elastic energy spatial zoning evolution model of surrounding rock under different driving speeds. Yang et al. [10] divided the rock burst roadway into a head-on area, dynamic evolution area of a plastic circle, and stable area of a plastic circle. Li et al. [11] divided the rectangular roadway roof into fracture through the area, fracture development area, microfracture area, and nonfracture area. Yu et al. [12] studied the loose range of rectangular roadway surrounding rock under different lithologic conditions by combining the method of multipoint displacement of deep base point and borehole peeping. Yu et al. [13] studied the distribution and evolution law of stress, displacement, and plastic zone of a roadway with a composite roof. Pan et al. [14] studied the stress distribution, surrounding rock displacement, and plastic zone distribution characteristics of the bottom gas drainage roadway through numerical simulation. Meng et al. [15] obtained the evolution process of roadway surrounding rock impact by studying the stress, displacement, and plastic zone distribution of soft rock roadway. Wang et al. [16] studied the analytical expressions of stress distribution, plastic zone, and disturbed zone width on both sides of the roadway in a gas coal seam. Hou et al. [17] studied the deformation characteristics and acoustic emission characteristics of rectangular roadway surrounding rock under different initial in situ stresses through a laboratory test. Yin et al. [18] studied the critical plastic softening zone depth and critical load of the rectangular roadway under rock burst. Rock burst occurs when the softening zone of tunnel rock mass with rock burst tendency reaches the critical depth [19]. Li et al. [20] studied the deformation and failure process of rectangular roadways through numerical simulation and field observation. Zheng et al. [21] analyzed the calculation formula of the Hoek Brown constitutive model based on the stress of rectangular roadways and studied the effect of anchorage system on roadway roof under different preloads. Chen et al. [22] studied the working face stability of shallow buried square tunnels in heterogeneous soil. Zhao et al. [23] applied the theory of complex variable function to solve the stress of square tunnel surrounding rock in a homogeneous isotropic elastic rock mass. Zhang et al. [24] established the friction work calculation model of roadway plastic zone and studied the influence of the relationship between total energy and friction work in roadway impact area on rock burst. Yi et al. [25] studied the transmission and dissipation of strain energy in the surrounding rock of deep roadway by numerical simulation. Wen et al. [26] studied the rock burst evaluation method based on the ratio of released energy to the absorbed energy. However, the research on the law of plastic zone evolution and energy dissipation around square roadway needs to be further studied.

In this paper, the rotational square expansion plastic zone evolution model of square roadway was established, and the shear slip stress conditions of square roadway based on the theory of complex variable function are studied. The stress distribution, plastic zone expansion, elastic energy density, local energy release rate, and total energy released by surrounding rock are analyzed, and the optimization scheme of the roadway section is proposed.

2. Roadway Shear Slip Impact Model and Surrounding Rock Stress Distribution

2.1. Shear Slip Impact Model of Roadway. After the excavation of the square roadway, the high-stress concentration is formed at the corner, and the shear slip occurs and expands continuously from the corner, as shown in Figure 1. When the shear slip zone passes through, a square failure zone is formed, which is called square failure zone I. After the formation of square failure zone I, the stress concentration zones shift from the corners of the roadway to the corners of square failure zone I. And the shear slip continued to expand in a square form from the corners of square failure zone I, forming square failure zone II. Either square failure zone is circumscribed with the tunnel contour (or the previous square failure zone) and rotated 45°, and the expansion of plastic failure area is called rotational square expansion, and the shear slip line field is rotational square slip line field.

After the formation of square failure zone II, the stress distribution at the corner of square failure zone II changes due to the reaction of the destroyed coal and rock mass in the roadway. The shear failure does not propagate according to the rotational square but tends to the logarithmic spiral [27, 28] shear slip mode.

When the roadway failure does not form square failure zone I, the plastic zone is small and will not form a large-scale rock burst. When the roadway failure forms square failure zone I, the failure area is connected for the first time, forming a large range of overall weak blocks. If there are high elastic energy accumulations around the roadway, it is easy to form a large-scale roadway rock burst. The center of two sides, roof, and floor are the main impact areas, while the impact at the corner is weak. When the roadway failure forms square failure zone II, the overall weak block of the surrounding rock further increases, which is easy to form large-scale roadway rock burst. The two sides, roof, floor, and corners are the main impact areas.

2.2. Stress Distribution and Impact Determination of Surrounding Rock Based on Complex Function Theory. In [23], the stress distribution of square roadway surrounding rock is studied by complex variable function and integral transformation theory. The circular stress distribution function of surrounding rock in polar coordinates of square roadway is given as follows:

$$\sigma_\theta = 4P\left(\frac{AB + C\ D}{B^2 + D^2} - \frac{1}{4}\right) + 4\lambda P\left(\frac{BE + DF}{B^2 + D^2} - \frac{1}{4}\right), \quad (1)$$

where $A = (6/53)\cos 4\ \theta + (3328/395)\cos 2\ \theta - 4$, $B = \cos 8\ \theta - 4\theta - 8$, $C = (6/53)\sin 4\ \theta + (3328/395)\sin 2\ \theta$, $D = \sin 8\ \theta - 4 \sin 4\ \theta$, $E = (6/53)\cos 4\ \theta + (3328/395)\ \cos 2\ \theta - 4$, $F = (6/53)\ \sin 4\ \theta + (3328/395)\sin 2\ \theta$, P is the

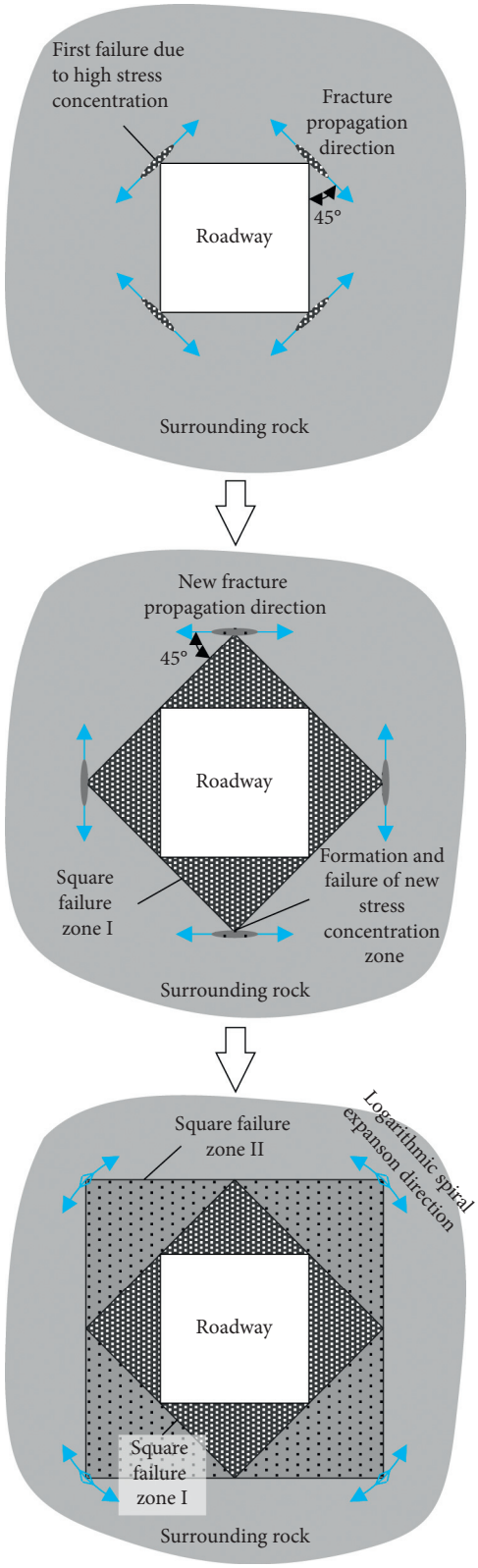

Figure 1: Evolution model of roadway failure area.

original rock stress along the X-axis direction, λ is the stress ratio along Y-axis to the x-axis, and θ is the polar angle.

The length of the roadway is much larger than the cross section of the roadway. The deformation and failure of the roadway can be approximated as a plane strain problem. According to the plane strain characteristics, equation (2) can be obtained by universal Hooke's law.

$$\sigma_z = \frac{1}{2}(\sigma_\theta + \sigma_r), \tag{2}$$

where σ_z is the stress along the length of the roadway and σ_r is the radial stress of the roadway.

σ_r is 0 on the surface of the roadway, and σ_m, which is the average stress of roadway, is as follows:

$$\sigma_m = \frac{1}{3}(\sigma_\theta + \sigma_r + \sigma_z) = \frac{1}{2}\sigma_\theta. \tag{3}$$

According to the characteristics along the slip line, $\Delta\sigma_m$ is directly proportional to $\Delta\omega$.

$$\Delta\sigma_m = \begin{cases} 2k\Delta\omega, & \text{Group } \alpha, \\ -2k\Delta\omega, & \text{Group } \beta, \end{cases} \tag{4}$$

where $\Delta\sigma_m$ is the average stress change in the same slip line, $\Delta\omega$ is the angle of slip line, k is the radius of the stress circle, and α and β are group α and group β of slip lines, respectively.

The slip line between corners of square failure zone I and square failure zone II are straight line segments, and $\Delta\omega$ is 0. The average stress in a linear interval of the slip line is equal, while $\Delta\sigma_m$ is 0. Average stresses of the slip line in square failure zone I and square failure zone II are equal because linear intervals are connected.

The average stress equation of slip line can be obtained from equations (1), (3), and (4):

$$\sigma_m = \begin{cases} \frac{1}{2}\sigma_\theta|_{\theta=(\pi/4)}, & \text{linear interval}, \\ \frac{1}{2}\sigma_\theta + 2k\Delta\omega'|_{\theta=(\pi/4)}, & \text{group } \alpha, \\ \frac{1}{2}\sigma_\theta - 2k\Delta\omega'|_{\theta=(\pi/4)}, & \text{group } \beta, \end{cases} \tag{5}$$

where $\Delta\omega'$ is the angle from the starting point of a spiral line to any point of the spiral line.

According to the Mohr-Coulomb criterion, under the limit equilibrium state, the stress state at any point can be expressed as

$$\begin{cases} \sigma = \sigma_m + k\cos\left(\frac{\pi}{2} + \varphi\right), \\ \tau = k\sin\left(\frac{\pi}{2} + \varphi\right), \end{cases} \tag{6}$$

where σ is the normal stress, τ is the shear stress, and φ is the internal friction angle.

Substituting equation (5) into equation (6), the stress state at any point in the limit equilibrium state is equation (7). When the stress state of the surrounding rock breaks through the limit equilibrium state, the shear slip impact occurs in the corresponding region.

$$\begin{cases} \sigma = \begin{cases} \dfrac{1}{2}\sigma_\theta + k\cos\left(\dfrac{\pi}{2}+\varphi\right)\Big|_{\theta=(\pi/4)}, & \text{linear interval,} \\ \dfrac{1}{2}\sigma_\theta + 2k\Delta\omega' + k\cos\left(\dfrac{\pi}{2}+\varphi\right)\Big|_{\theta=(\pi/4)}, & \text{group } \alpha, \\ \dfrac{1}{2}\sigma_\theta - 2k\Delta\omega' + k\cos\left(\dfrac{\pi}{2}+\varphi\right)\Big|_{\theta=(\pi/4)}, & \text{group } \beta, \end{cases} \\ \tau = k\sin\left(\dfrac{\pi}{2}+\varphi\right). \end{cases} \tag{7}$$

3. Numerical Simulation of Failure Law of Square Roadway

3.1. Modeling. The strain-softening model was established by FLAC^{3D} software. The model length × width × height is 100 m × 1 m × 50 m. The physical and mechanical parameters of rock strata are mainly taken from Xinjulong Coal Mine, and the conventional parameters are used to supplement the missing coal and rock parameters. Table 1 lists the physical and mechanical parameters of each rock stratum.

Fix the bottom and lateral boundaries, and apply different forces on the top of the model, respectively. 21 groups of different initial stress states are formed, and the vertical stress at the boundary between the coal seam and roof is 1.0–3.0 [σ_c], respectively (the ratio of vertical stress to uniaxial compressive strength Ic = 1.0–3.0). The coefficient of lateral pressure is 1.0.

3.2. Law of Stress Change. After the model is balanced, the roadway is excavated along the coal seam floor with a section size of 4 m × 4 m. Four vertical stress measuring points are arranged in the far field of the roadway sidewall to monitor the change of regional stress. The distance between the stress measuring point and the roadway sidewall is 28–37 m, and the vertical direction is located on the horizontal plane of the middle point of the roadway. When Ic = 1.5, the vertical stress change of each measuring point is shown in Figure 2. Each measuring point has experienced two obvious stress reduction and recovery stages, which indicates that the surrounding rock of the roadway has a twice obvious failure, causing regional stress adjustment.

The evolution of compressive stress concentration area of roadway surrounding rock is shown in Figure 3. When the roadway is just excavated, the compressive stress is concentrated near the four corners of the roadway. After the first obvious failure of the roadway, the compressive stress concentration area rotates 45° and expands outward. After the second obvious failure of the roadway, the compressive stress concentration area rotated 45° again and expanded outward.

3.3. Evolution Law of Failure Area. When Ic = 1.5, the plastic zone expansion of the surrounding rock is shown in Figure 4. After the first obvious failure of the roadway, square failure zone I is formed, and square failure zone I is mainly shear and tensile failure. After the second obvious failure of the roadway, square failure zone II is formed, and square failure zone II is mainly shear failure. The main shear failure areas of the surrounding rock are shown in Figure 5, and the main shear failure zones extend in a rotating square shape.

When Ic = 1.5, the shear strain nephogram of the roadway surrounding rock is shown in Figure 6. The shear strain is the largest at the four corners of the roadway, and a square shear slip line field connected with the roadway and rotated 45° is formed, which is the boundary of square failure zone I in the theoretical analysis, and square failure zone II with a rotation of 45° is formed outside square failure zone I.

When the original rock stress is low, the surrounding rock tends to be stable after the formation of square failure zone II. When the original rock stress is high, after the formation of square failure zone II, the failure area continues to expand outward, as shown in Figure 7, which shows the shear strain nephogram of surrounding rock with Ic = 3.0. After the formation of square failure zone II, the stress distribution has changed, and the propagation direction of the failure zone has changed. The slip line field is similar to the spiral expansion form.

4. Energy Dissipation Mechanism of Square Roadway

4.1. Energy Monitoring Methods. When the elastic moduli of the three principal stress directions are the same, the elastic strain energy released by the element can be expressed as [29, 30]

$$U^e = \frac{1}{2E_0}\left[\sigma_1^2 + \sigma_2^2 + \sigma_3^2 - 2\nu\left(\sigma_1\sigma_2 + \sigma_2\sigma_3 + \sigma_1\sigma_3\right)\right], \tag{8}$$

where U^e is the elastic strain energy released by the element, E_0 is the elastic modulus, σ_1, σ_2, and σ_3 are the three principal stresses of the element, and ν is the Poisson ratio.

The elastic strain energy released by the element is expressed by the local energy release rate (LERR), and the sum of elastic strain energy released by all elements is the total energy released by the surrounding rock, which is recorded as ERE. The calculation method is as follows [31]:

$$\mathrm{LERR}_i = U^e_{i\max} - U^e_{i\max}, \tag{9}$$

$$\mathrm{ERE} = \sum_{i=1}^{n}\left(\mathrm{LERR}_i \cdot V_i\right), \tag{10}$$

where LERR_i is the local energy release rate of the ith element and $U^e_{i\max}$ is the peak value of elastic strain energy

Table 1: Model parameters in the FLAC^{3D} model.

Layers	Lithology	Thickness (m)	Elastic modulus (GPa)	Poisson ratio	Tensile strength (MPa)	Cohesion (MPa)	Internal friction angle(°)
Roof2	Fine sandstone	16	50.69	0.3	7.78	5	35
Roof1	Siltstone	4	21.37	0.3	2.92	5	35
Seam	Coal	7	17.04	0.37	0.74	3.1	28.5
Floor	Fine sandstone	23	19.68	0.3	4.99	5	35

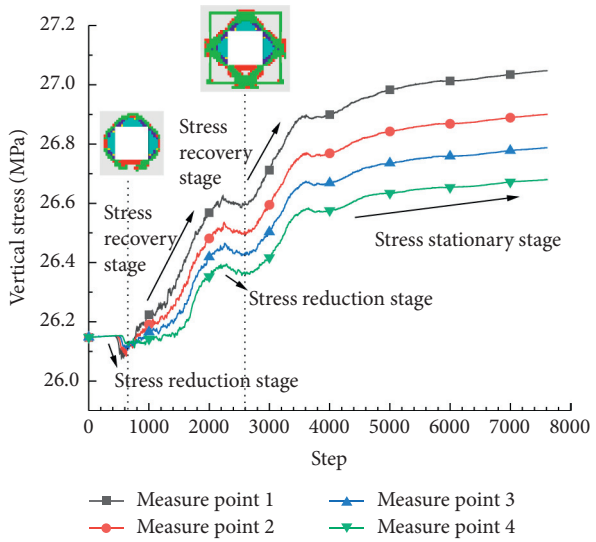

Figure 2: Regional vertical stress monitoring curve.

density of the ith element before failure. $U^e_{i\,\min}$ is the valley value of elastic strain energy density after the failure of the ith element and V_i is the volume of the ith unit.

According to the above method, FLAC^{3D} software is used to program Fish language to monitor the energy parameters of the model.

4.2. Energy Evolution Law. When $Ic = 1.5$, the evolution law of elastic energy density of surrounding rock is shown in Figure 8. After the formation of square failure zone I, the elastic energy accumulates at its four corners. After the formation of square failure zone II, the elastic energy accumulated at the four corners of square failure zone II.

When $Ic = 1.5$, the local energy release rate of the surrounding rock is shown in Figure 9. Four corners of the roadway and the four corners of square failure zone I are the areas where a lot of energy is released. The maximum local energy release rate is 30.6 kJ/m^3.

When $Ic = 1.5$, the total energy release curve of the surrounding rock is shown in Figure 10. There are two peaks in the total energy released by the surrounding rock. When the total energy released by the surrounding rock reaches the peak value I, the square failure zone I is basically formed. The surrounding rock tends to be stable and the stress is readjusted, resulting in the accumulation of new strain energy, which leads to the decrease of the total energy released in the region. When the total energy released by the surrounding rock reaches peak II, the square failure zone II is basically formed. The stress is adjusted again, and the surrounding rock tends to the final stable state and the total energy released tends to be stable.

The statistical results of maximum elastic energy density (PE) and local energy release rate (LERR) of each model are shown in Figure 11. Through data fitting, it can be seen that PE and LERR increase exponentially with Ic.

5. Engineering Verification

5.1. Case 1. Liangbaosi Coal Mine is located in Juye coalfield. The average buried depth of 3507 working face is 1067 m, and the average thickness of the coal seam is 6.2 m. The coal seam, roof, and floor have a weak impact tendency. A coal blasting occurred during the tunneling of the 3507 track gateway, which resulted in roof subsidence of the right shoulder and bolt fracture, as shown in Figure 12. The roof subsidence of the right shoulder of the roadway is 200–300 mm, while the middle part of the roof has no deformation, which is consistent with the theoretical analysis that the corner of the roadway is damaged first.

5.2. Case 2. Xinjulong Coal Mine is located in the south-central part of Juye coalfield. The average buried depth of the 2305s fully mechanized caving face is 1004 m. At present, the thickness of the coal seam in the mining area is 8.1–10.5 m,

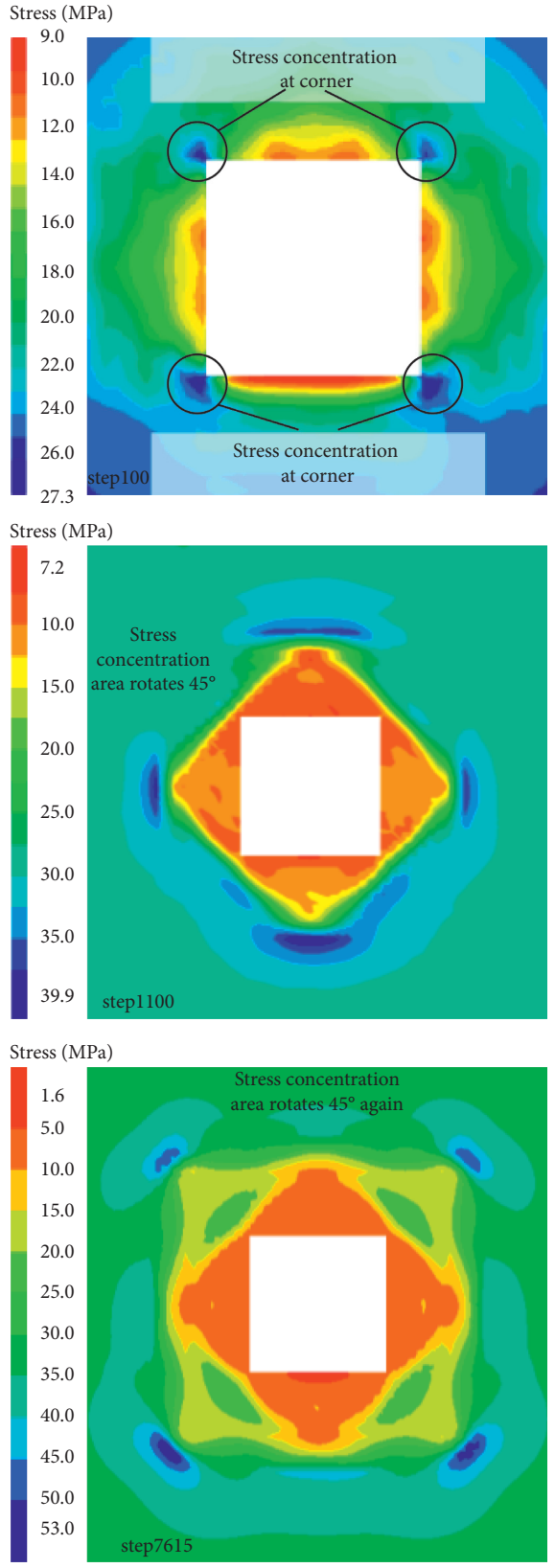

Figure 3: Evolution of compressive stress concentration.

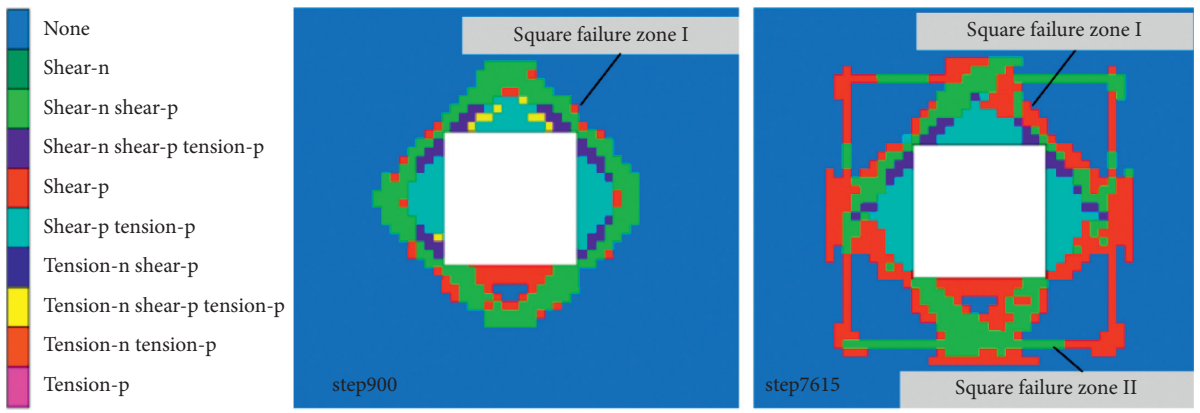

Figure 4: Evolution of plastic zone of the surrounding rock.

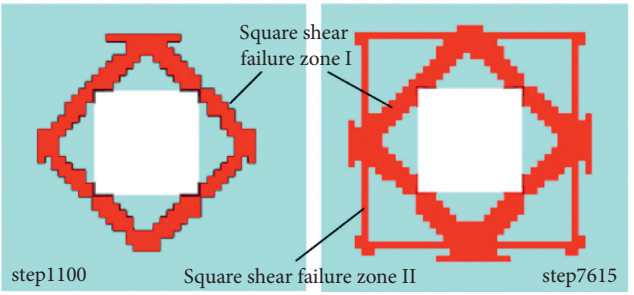

Figure 5: Evolution of main shear failure area of surrounding rock.

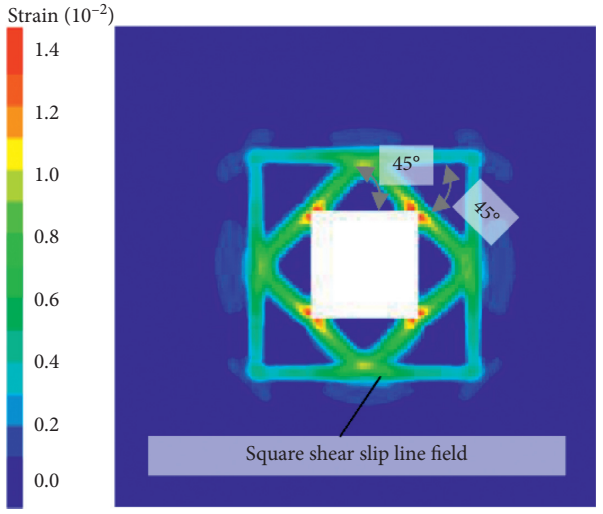

Figure 6: Nephogram of the shear strain of surrounding rock ($Ic = 1.5$).

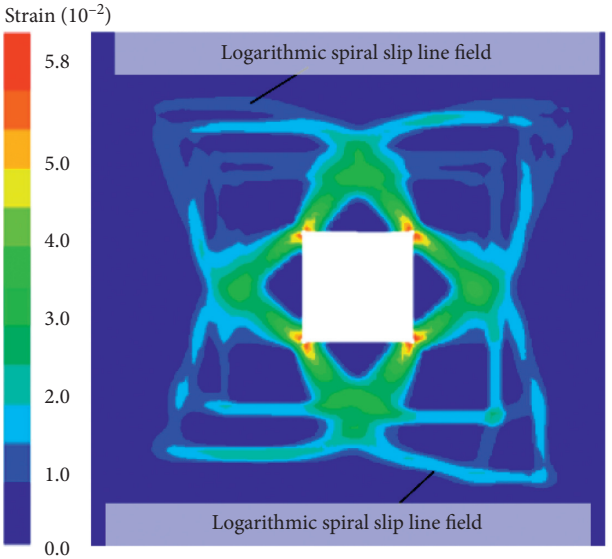

Figure 7: Nephogram of the shear strain of surrounding rock ($Ic = 3.0$).

and the coal seam and roof have a weak impact tendency. On February 22, 2020, a rock burst occurred in the 2305s upper drift and associated roadway. The situation after impact in some areas is shown in Figure 13. The middle part of the sides and the middle part of the roof protrude. The deformation of roadway corners is relatively small. It is consistent with the theoretical analysis that the main impact areas are the roadway side and middle roof.

6. Optimization of Roadway Section

The right angle in the structure is easy to produce stress concentration, while the fillet stress concentration is low. The filleted corner should be kept as far as possible in the roadway excavation. The roadway driving along the bottom shall avoid forming a right angle at the top angle, while the

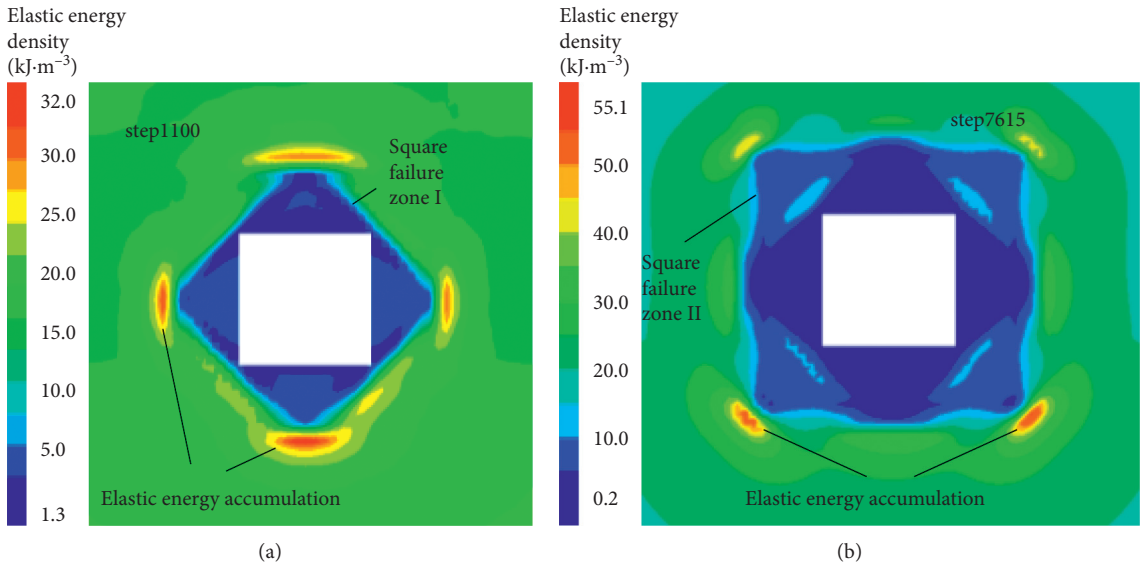

Figure 8: Evolution of elastic energy density of surrounding rock.

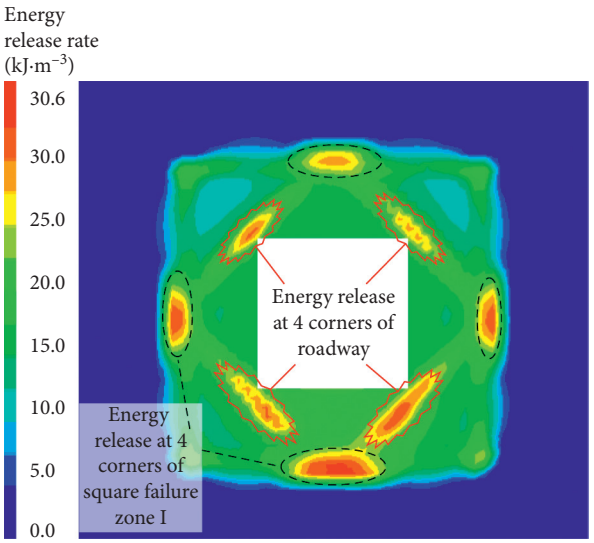

Figure 9: Nephogram of local energy release rate of surrounding rock.

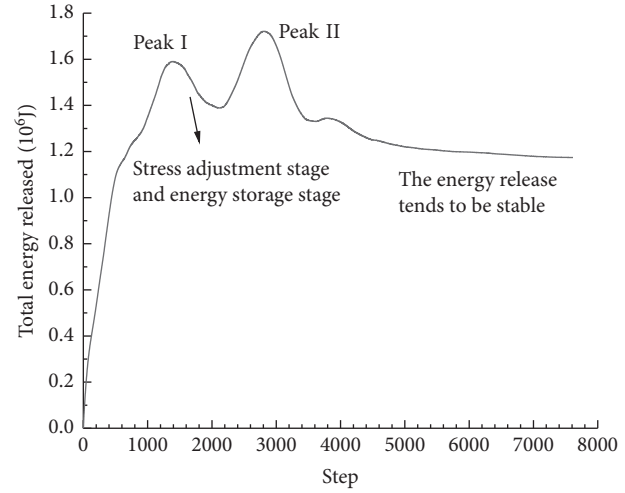

Figure 10: Curve of the total energy released from surrounding rock.

roadway driving along the top shall avoid forming a right angle at the bottom angle.

The two roof corners of the roadway in the model, where $Ic = 1.5$, are changed into rounded corners, and the fillet radius is 0.5 m. When the model is recalculated, the law of plastic zone expansion has changed. The surrounding rock forms an arch failure area. The newly formed arched surrounding rock structure can bear more force and reduce deformation. As shown in Figures 14 and 15, the maximum depth of the plastic zone on the roof of the fillet roadway is reduced by 20%, the maximum depth of plastic zone on both sides is reduced by 10%, and the maximum horizontal displacement is moved from the middle point of the two sides to the bottom angle of the two sides.

Figure 16 shows the cloud chart of the maximum elastic energy density after roadway excavation. The maximum elastic energy density of the square roadway is 61.7 kJ/m^3, which is located on the roadway floor. The maximum elastic energy density of the round corner roadway is 48.2 kJ/m^3, which is located at the top coal of the roadway. The maximum elastic energy density of the filleted corner roadway is 22% less than that of the square roadway, and the location of the maximum elastic energy density is transferred from the floor to the top coal.

Figure 17 shows the local energy release rate nephogram of the round corner roadway. The energy release rate and range of the floor are larger than those of top coal. The corners of the roadway floor are still right angle, and the plastic zone still expanded in a rotating square shape in the early stage. A large amount of energy is released at the corner of square failure zone I. When the corners of the roadway roof are changed to round corners, the plastic zone of the

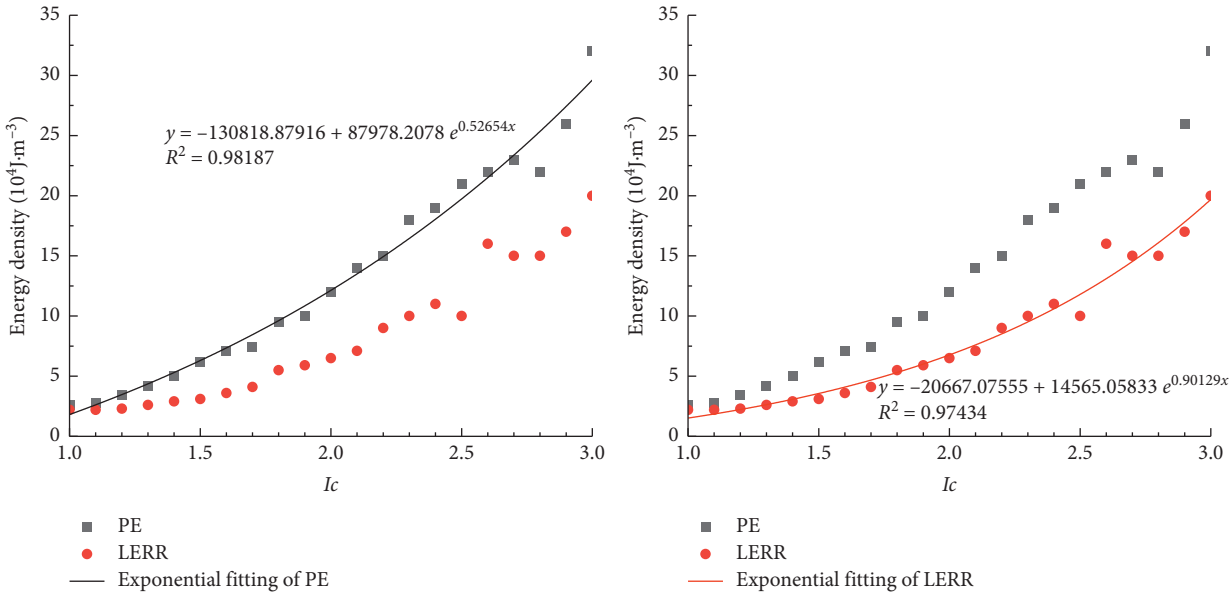

Figure 11: Statistical chart of maximum elastic energy density and local energy release rate.

Figure 12: Drawing of roof subsidence at the right shoulder of the roadway.

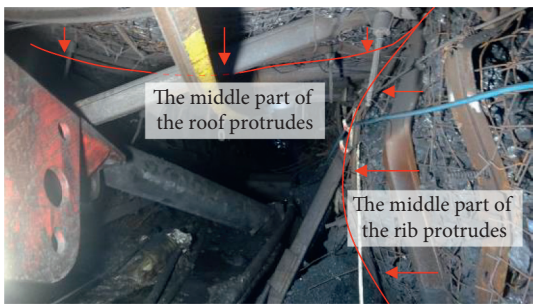

Figure 13: Upper drift impact damage diagram.

roof expands to form an arch structure, which increases the bearing capacity and releases less energy. Therefore, the accumulated elastic energy of the floor is less than that of the roof, but a greater energy release and damage occur. At the same time, it can be determined that the ability of top coal with arch structure is higher than that of floor sandstone with right angle corner.

7. Discussion

This paper studies the impact failure mechanism of the square roadway under high stress. The roadway mainly

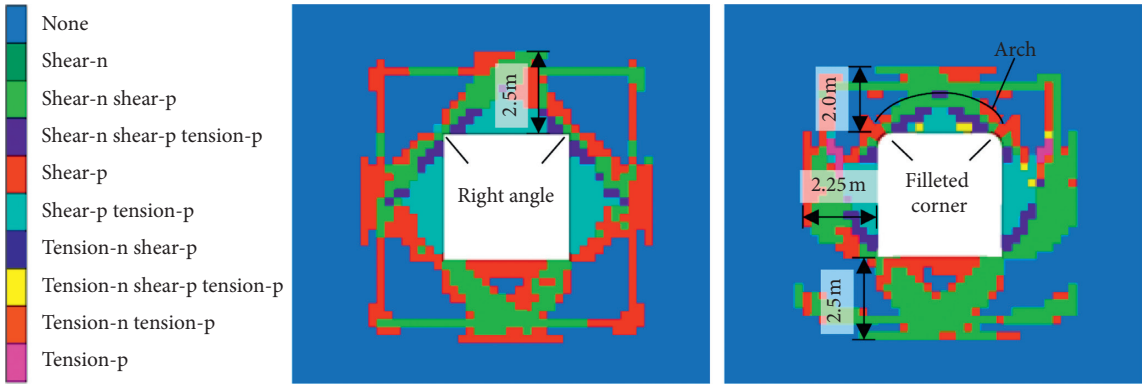

Figure 14: Comparison of the plastic zone of the roadway.

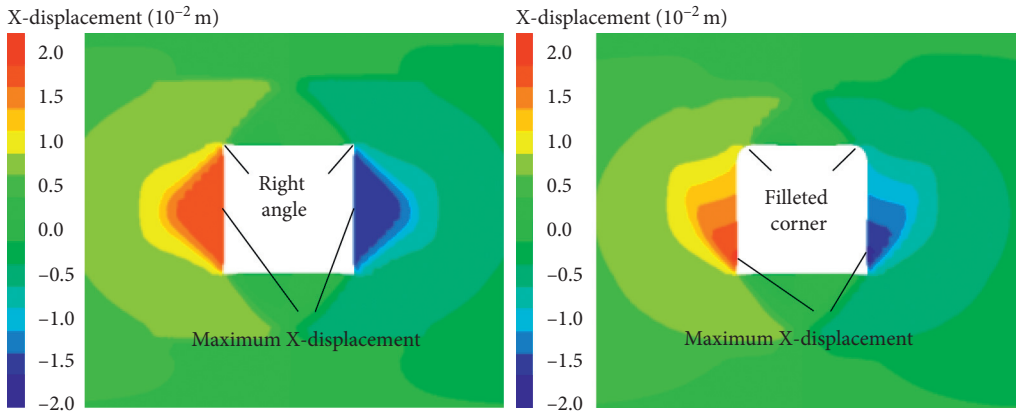

Figure 15: Comparison of horizontal displacement of the roadway.

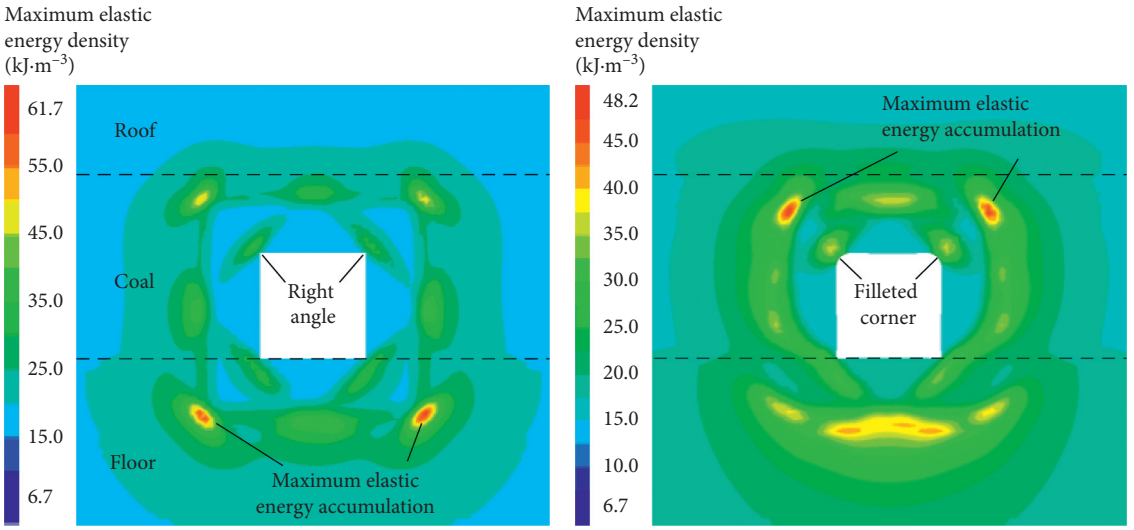

Figure 16: Comparison of maximum elastic energy density.

presents tensile shear failure. The shear failure starts from the four corners of the roadway, develops at 45° with the roadway contour, and finally integrates into a square shear failure area, which is connected with the roadway contour and rotated 45° to the roadway contour. Then, the four corners of the square shear failure zone begin to expand, forming a new square shear failure zone, which is connected with the original square shear failure zone and rotated 45° to form a rotating square slip line field. After two times of rotation square shear failure, the stress distribution at the corner changed due to the reaction of the damaged coal and rock mass in the roadway. The shear

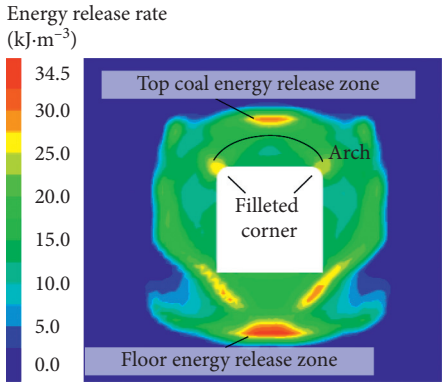

Figure 17: Nephogram of the local energy release rate of filleted corner roadway.

failure does not expand in the form of rotation square, and the expansion form of shear failure tends to logarithmic spiral shear slip, which is similar to the spiral shear slip line studied by scholars before.

When the corners of the square roadway are changed into rounded corners, the evolution law of the plastic zone changes, and the square plastic zone is transformed into an arch shape, which is more conducive to bearing capacity and can reduce the accumulation of elastic energy of surrounding rock. In addition, the construction of shear bolts in the main shear area of the roadway can strengthen the ability of the roadway to withstand shear failure. More prevention and control technologies need more in-depth research.

The research results enrich the failure mechanism of roadway sliding and impact and can provide a basic theoretical reference for the design of new roadway cross section and support forms based on rock burst prevention and control.

8. Conclusions

In this paper, the rotational square expansion plastic zone evolution model of square roadway was established, and the stress criterion of shear slip impact of square roadway based on complex function theory is given.

When the roadway is just excavated, the compressive stress is concentrated near the four corners of the roadway, and the main shear failure starts from the four corners and gradually forms the square failure zones I and II. Square failure zone I is connected with the roadway contour and rotated by 45°, and square failure zone II is connected with square failure zone I and rotated 45°. When the original rock stress is low, after the formation of square failure zone II, the surrounding rock tends to be stable, forming a rotating square shear slip line field. When the original rock stress is high, the shear failure of the surrounding rock continues to occur after the formation of square failure zone II and tends to expand in the form of a logarithmic spiral.

When square failure zone I is not formed, the plastic zone is small and large-scale rock burst will not occur. When square failure zone I is formed, the failure area is connected for the first time, forming a large-scale overall weak block. If there is a high elastic energy accumulation around the roadway, it is easy to form a large-scale roadway rock burst. The center of two sides and the center of roof and floor are the main impact areas, and the impact at each corner is weak. When square failure zone II is formed, the weak block of surrounding rock of roadway will further increase, which is easy to form large-scale roadway rock burst. The two sides, roof, and floor and corners of the roadway are the main impact areas.

The corners of the square roadway and the corners of square failure zones I and II are the main energy accumulation and release areas. The maximum elastic energy density and local energy release rate increase exponentially with the ratio of vertical stress to uniaxial compressive strength. When the corners of the roof are changed to round corners, the plastic zone of the roof expands to form an arch structure, the bearing capacity increases, and the plastic zone becomes smaller when it reaches stability. The maximum elastic energy density of the round corner roadway is 22% less than that of the square roadway, which reduces the energy level and possibility of rock burst.

Data Availability

The data used to support the findings of this study are available from the corresponding author upon request.

Conflicts of Interest

The authors declare that there are no conflicts of interest regarding the publication of this paper.

Acknowledgments

This research was supported by the National Natural Science Foundation of China (Grant nos. 51634001 and 51904017), Major Scientific and Technological Innovation Projects in Shandong Province (Grant no. 2019SDZY02), the Fundamental Research Funds for the Central Universities (Grant no. FRF-TP-20-002A2), and Project funded by China Postdoctoral Science Foundation (Grant no. 2020M682214). The authors would like to thank all members in Shandong Energy Group Co., LTD., for their help with the fieldwork.

References

[1] C. Wang, A. Cao, C. Zhang, and I. Canbulat, "A new method to assess coal burst risks using dynamic and static loading analysis," *Rock Mechanics and Rock Engineering*, vol. 53, no. 3, pp. 1113–1128, 2020.

[2] J. Zhang, Y. Wang, Y. Sun, and G. Li, "Strength of ensemble learning in multiclass classification of rockburst intensity," *International Journal for Numerical and Analytical Methods in Geomechanics*, vol. 44, no. 13, pp. 1833–1853, 2020.

[3] Y. Chen, D. Li, F. Jiang et al., "Use of the equivalent mining height method for understanding overlying strata movement and stress distribution in an isolated coal pillar," *Shock and Vibration*, vol. 2020, Article ID 8820886, 12 pages, 2020.

[4] D. Ge, F. Jiang, D. Li, C. Wang, and Y. Chen, "Floor burst mechanism and roadway layout optimization under the

influence of coal pillar," *Journal of Mining & Safety Engineering*, vol. 37, no. 2, pp. 282–288, 2020.

[5] G. Shi, J. Zhu, B. LI, and J. Yang, "Elastic analysis of hole-edge stress of rectangular roadway," *Rock and Soil Mechanics*, vol. 35, no. 9, pp. 2587–2593, 2014.

[6] X. Guo, Z. Zhao, X. Gao, Z. Ma, and N. Ma, "The criteria of underground rock structure failure and its implication on rockburst in roadway : a numerical method," *Shock and Vibration*, vol. 2019, Article ID 7509690, 12 pages, 2019.

[7] W. Wu, F. Gong, and W. Yang, "Experimental simulation study of spalling in deep rectangular tunnel with plastic fine grain marble," *Tunnelling and Underground Space Technology*, vol. 98, Article ID 103319, 2020.

[8] X. Wang, F. Tian, X. Bai, and X. Guo, "Numerical simulation on the deformation-cracking process of rectangular tunnel surrounding rock under different impact velocities," *Journal of Vibration and Shock*, vol. 39, no. 14, pp. 94–108, 2020.

[9] S. Wang, W. Ju, J. Pan, and C. Lu, "Mechanism of energy partition evolution of excavation roadway rockburst in coal seam under tectonic stress field," *Journal of China Coal Society*, vol. 44, no. 7, pp. 2000–2010, 2019.

[10] G. Yang, F. Jiang, X. Qu et al., "Comprehensive monitoring and early warning technology for rock burst of tunneling face with thick coal seams," *Chinese Journal of Geotechnical Engineering*, vol. 41, no. 10, pp. 1949–1958, 2019.

[11] Q. Li, J. Hou, T. Han, H. Liu, and S. Wang, "Failure characteristics and support technique of surrounding rock for deep rectangular roadway in Yangzhuang mine," *Journal of China University of Mining & Technology*, vol. 45, no. 6, pp. 1124–1131, 2016.

[12] Y. Yu and S. Gu, "Measurement of loosened surrounding rock scope in the rectangular roadway and its control techniques research," *Journal of Mining & Safety Engineering*, vol. 30, no. 6, pp. 828–835, 2013.

[13] Y. Yu, X. Wang, J. Bai, L. Zhang, and H. Xia, "Deformation mechanism and stability control of roadway surrounding rock with compound roof: research and applications," *Energies*, vol. 13, no. 6, p. 1350, 2020.

[14] R. Pan, Z. Ma, M. Yu, and S. Wu, "Research on the deformation characteristics and support technology of a bottom gas extraction roadway under repeated interference," *Advances in Civil Engineering*, vol. 2019, Article ID 1413568, 14 pages, 2019.

[15] Q. Meng, L. Han, Y. Xiao, H. Li, S. Wen, and J. Zhang, "Numerical simulation study of the failure evolution process and failure mode of surrounding rock in deep soft rock roadways," *International Journal of Mining Science and Technology*, vol. 26, no. 2, pp. 209–221, 2016.

[16] G. Wang, R. Wang, M. Wu, C. Fan, and X. Song, "Strength criterion effect of the translator and destabilization model of gas-bearing coal seam," *International Journal of Mining Science and Technology*, vol. 29, no. 2, pp. 327–333, 2019.

[17] G. Hou, H. Jing, J. Liang et al., "Experimental study on surrounding rock deformation and acoustic emission characteristics of rectangular roadway under different loads," *Rock and Soil Mechanics*, vol. 46, no. 6, pp. 1818–1828, 2020.

[18] W. Yin, Y. Pan, and Z. Li, "Mechanism of rock burst in rectangular section roadway," *Chinese Journal of Geotechnical Engineering*, vol. 40, no. 6, pp. 1135–1142, 2018.

[19] Y. Pan, Y. Zhang, and G.-M. Yu, "Mechanism and catastrophe theory analysis of circular tunnel rockburst," *Applied Mathematics and Mechanics*, vol. 27, no. 6, pp. 841–852, 2006.

[20] T. Li, Z. Lu, J. Liu, and X. Ma, "Deformation and failure process analysis of rectangular roadway in muddy weakly cemented soft rock strata," *Rock and Soil Mechanics*, vol. 35, no. 4, pp. 1077–1083, 2014.

[21] X. Zheng, L. Zhang, N. Zhang, and N. Liu, "Pre-stressed anchorage function and evolution in the roof of rectangular roadway in deep mine," *Journal of China University of Mining & Technology*, vol. 42, no. 6, pp. 929–934, 2013.

[22] G. Chen, J. Zou, Q. Min, W. Guo, and T. Zhang, "Face stability analysis of a shallow square tunnel in non-homogeneous soils," *Computers and Geotechnics*, vol. 114, Article ID 103112, 2019.

[23] G. Zhao and S. Yang, "Analytical solutions for rock stress around square tunnels using complex variable theory," *International Journal of Rock Mechanics and Mining Sciences*, vol. 80, pp. 302–307, 2015.

[24] J. Zhang, F. Jiang, J. Yang, W. Bai, and L. Zhang, "Rockburst mechanism in soft coal seam within deep coal mines," *International Journal of Mining Science and Technology*, vol. 27, no. 3, pp. 551–556, 2017.

[25] K. Yi, Z. Liu, Z. Lu, Y. Zhang, and Z. Sun, "Transfer and dissipation of strain energy in surrounding rock of deep roadway considering strain softening and dilatancy," *Energy Science & Engineering*, vol. 9, no. 1, pp. 27–39, 2021.

[26] Z. Wen, X. Wang, Y. Tan et al., "A study of rockburst hazard evaluation method in coal mine," *Shock and Vibration*, vol. 2016, Article ID 8740868, 9 pages, 2016.

[27] B. Meng, H. Jing, K. Chen et al., "Shear and slip failure mechanism and control of tunnels with weak surrounding rock," *Chinese Journal of Geotechnical Engineering*, vol. 34, no. 12, pp. 2255–2262, 2012.

[28] F. Luo, B. Yang, L. Sun et al., "Experimental research on the failure characteristics of surrounding rock under high vertical ground stress," *Journal of Mining & Safety Engineering*, vol. 29, no. 4, pp. 497–504, 2012.

[29] H. Xie, Y. Ju, and L. Li, "Criteria for strength and structural failure of rocks based on energy dissipation and energy release principles," *Chinese Journal of Rock Mechanics and Engineering*, vol. 24, no. 17, pp. 3003–3010, 2005.

[30] D. Ge, D. Li, F. Jiang et al., "Reasonable pressure-relief borehole spacing in coal of different strength," *Journal of Mining & Safety Engineering*, vol. 37, no. 3, pp. 578–585+593, 2020.

[31] G. Su, X. Feng, Q. Jiang, and G. Chen, "Study on new index of local energy release rate for stability analysis and optimal design of underground rockmass engineering with high geostress," *Chinese Journal of Rock Mechanics and Engineering*, vol. 25, no. 12, pp. 2453–2460, 2006.